


ARTICLE

Fluid shear stress stimulates breast cancer cells to display invasive and chemoresistant phenotypes while upregulating *PLAU* in a 3D bioreactor

Caymen M. Novak¹ | Eric N. Horst^{1,2} | Charles C. Taylor¹ | Catherine Z. Liu¹ |
Geeta Mehta^{1,2,3} ¹Department of Biomedical Engineering,
University of Michigan, Ann Arbor, Michigan²Department of Materials Science and
Engineering, University of Michigan, Ann
Arbor, Michigan³Macromolecular Science and Engineering,
University of Michigan, Ann Arbor, Michigan**Correspondence**Dr. Geeta Mehta Department of Materials
Science and Engineering, Department of
Biomedical Engineering, Macromolecular
Science and Engineering, University of
Michigan, North Campus Research Complex
(NCRC), 2800 Plymouth Road, Building 28,
Room 3044W, Ann Arbor, MI 48109-2800.
Email: mehtagee@umich.edu**Funding information**Rivkin Center for Ovarian Cancer; Michigan
Ovarian Cancer Alliance (MIOCA);
Congressional Directed Medical Research
Programs, Grant/Award Numbers: W81XWH-
13-1-0134, W81XWH-16-1-0426; Center for
Scientific Review, Grant/Award Number:
P30CA046592; National Science Foundation,
Grant/Award Number: Graduate Research
Fellowship Grant No. 1256260**Abstract**

Breast cancer cells experience a range of shear stresses in the tumor microenvironment (TME). However most current in vitro three-dimensional (3D) models fail to systematically probe the effects of this biophysical stimuli on cancer cell metastasis, proliferation, and chemoresistance. To investigate the roles of shear stress within the mammary and lung pleural effusion TME, a bioreactor capable of applying shear stress to cells within a 3D extracellular matrix was designed and characterized. Breast cancer cells were encapsulated within an interpenetrating network hydrogel and subjected to shear stress of 5.4 dynes cm⁻² for 72 hr. Finite element modeling assessed shear stress profiles within the bioreactor. Cells exposed to shear stress had significantly higher cellular area and significantly lower circularity, indicating a motile phenotype. Stimulated cells were more proliferative than static controls and showed higher rates of chemoresistance to the anti-neoplastic drug paclitaxel. Fluid shear stress-induced significant upregulation of the *PLAU* gene and elevated urokinase activity was confirmed through zymography and activity assay. Overall, these results indicate that pulsatile shear stress promotes breast cancer cell proliferation, invasive potential, chemoresistance, and *PLAU* signaling.

KEYWORDS3D bioreactor, breast cancer, interpenetrating hydrogel, mechanotransduction, *PLAU*, shear stress

1 | INTRODUCTION

In 2018, breast cancer was the second leading cause of cancer-related death in females accounting for 30% of all new cancer diagnosis (Siegel, Miller, & Jemal, 2018). The progression of the disease is heavily dependent on the mammary tumor microenvironment (TME) which is comprised of a variety of dynamic stimuli, including shear, compression, tension and the surrounding three dimensional (3D) extracellular matrix (ECM) stiffness (Butcher, Alliston, & Weaver, 2009; DuFort, Paszek, & Weaver, 2011). To discover effective therapeutics, numerous in vitro models have been developed to isolate and explore the role of dynamic 3D stimuli within the TME (Bersini et al., 2014; Hylar et al., 2018; Li et al., 2011;

Polacheck, German, Mammoto, Ingber, & Kamm, 2014; Rijal & Li, 2016; Rizvi et al., 2015; Shieh, Rozansky, Hinz, & Swartz, 2011; Sung et al., 2013; Weigelt, Ghajar, & Bissell, 2014).

Breast cancer cells have been shown to alter their expression and behavior contingent on specialized cues originating from the surrounding microenvironment. For instance, it has been demonstrated that breast cancer cells show increased invasiveness when cultured in 3D versus 2D substrates (Sung et al., 2013; Weigelt et al., 2014) and promote motility, adhesion, and metastasis under shear stress (Avraham-Chakim et al., 2013; Avvisato et al., 2007; Mitchell & King, 2013a; 2013b; Swartz & Lund, 2012; Xiong et al., 2017). Cancer cells within primary tumors, pleural effusions, secondary metastasis, and the TME experience a wide range of shear stresses. Within the

primary tumor, interstitial fluid shear stress may be as low as $0.1 \text{ dynes cm}^{-2}$, but cancer cells exposed to vascular blood flow can experience fluid shear stress up to 30 dynes cm^{-2} (Barnes, Nauseef, & Henry, 2012; Harrell, Iritani, & Ruddell, 2007; Mitchell & King, 2013b; Shieh & Swartz, 2011; Weinbaum, Cowin, & Zeng, 1994). Interstitial velocity flow has been shown to stimulate rheotaxis within breast cancer cells, showing positive migration towards areas of elevated shear stress (Munson & Shieh, 2014; Polacheck, Charest, & Kamm, 2011; Polacheck et al., 2014). Breast cancer rheotaxis might be one mechanism guiding malignant tumor cells to distant metastatic sites. Fifty percent of all breast cancer patients present pleural effusions (Patil et al., 2015). Once advanced malignancies progress to pleural spaces, the cancer cells experience fluid shear stress ranging from $4.7 \text{ dynes cm}^{-2}$ to $18.4 \text{ dynes cm}^{-2}$, with maximum shear values reaching an excess of 60 dynes cm^{-2} (Waters, Glucksberg, Depaola, Chang, & Grotberg, 1996). Furthermore, changes in the extracellular fiber architecture, differences in ECM alignment, and expansion of the tumor itself alters the velocity and path of the fluid flow across the stimulated cells (Pedersen, Lichter, & Swartz, 2010). A rapidly changing TME both modulates and increases interstitial fluid flow over time within a diseased microenvironment. The continuous and elevated levels of shear stress present in the breast and malignant TME accentuates the importance of investigating the effects of shear forces within cancer progression (Pedersen, Boschetti, & Swartz, 2007; Pedersen et al., 2010; Shieh & Swartz, 2011).

Within the metastatic cascade of cancer, the urokinase plasminogen activator (uPA) system has been explicitly identified as an assistive mechanism (Mahmood, Mihalciou, & Rabbani, 2018). The uPA system aids in the degradation of surrounding ECM constructs allowing for enhanced cell migration and invasion. uPA is coded for by the Plasminogen Activator Urokinase (*PLAU*) gene and activates plasminogen via conversion to plasmin (Mahmood et al., 2018). Association between shear stress stimulus and the uPA system modulation has been shown for proximal tubular cells (Essig & Friedlander, 2003), endothelial cells (Diamond, Eskin, & McIntire, 1989; Dolan, Sim, Meng, & Kolega, 2012; Sokabe et al., 2004), and smooth muscle cells (Papadaki et al., 1998); although *PLAU* upregulation has been linked to metastatic cancers as a possible biomarker (Bredemeier et al., 2017; Sepiashvili et al., 2012; Tang & Han, 2013), it has yet to be directly tied to mechano-stimulus in cancer.

Several studies have investigated the effects of shear stress on various cancer types. Previously reported responses of cancer cells exposed to shear stress include increased chemoresistance, stem cell markers, viability, and changes in adhesion capability (Barnes et al., 2012; Ip et al., 2016; Zhao et al., 2014). Within breast cancer specifically, shear stress has been shown to modulate stemness (Triantafillu, Park, Klaassen, Raddatz, & Kim, 2017), survival (Regmi, Fu, & Luo, 2017), metastasis (Regmi et al., 2017), adhesion (Xiong et al., 2017; Zhao et al., 2014), pH regulation (Kawai, Kaidoh, Yokoyama, & Ohhashi, 2013), and motility (Yang et al., 2016) though the majority of these studies fail to account for the native 3D

microenvironment which significantly impacts cellular responses (Loessner et al., 2010; Weigelt et al., 2014). To more accurately probe the effects of shear stress on breast cancer, in vitro 3D models with shear stress stimulation are needed.

Here, we developed a bioreactor that stimulates breast cancer cells embedded in a 3D hydrogel matrix to pulsatile fluid flow allowing for tunable shear stress stimulation (Rotenberg, Ruvinov, Armoza, & Cohen, 2012). We utilized this 3D bioreactor to investigate the effects of shear stress on MDA-MB-231, MDA-MB-468, and MCF7 breast adenocarcinoma cells in a 3D pleural effusion TME. Through this 3D bioreactor, we identified consistent trends in shape factor alterations, proliferative tendencies, mechanotransduction, and chemoresistance in breast cancer cells exposed to shear stress. These findings suggest that breast cancer cells utilize the *PLAU* pathway for mechanotransduction of shear stress stimulus. The bioreactor is easily modifiable for a range of shear stresses, as well as, a variety of cancer cell types, making it a feasible platform for further investigation of shear stress in a variety of cancers.

2 | MATERIALS AND METHODS

2.1 | Materials and suppliers

2.1.1 | Cell culture, hydrogel polymerization, drugs, inhibitors, and assays

The following reagents required for cell culture were purchased from Gibco (Cleveland, TN): Dulbecco's Modified Eagle's medium (DMEM) growth medium (31-053-028), RPMI growth medium (11875119), antibiotic/antimycotic (15240062), 0.25% trypsin-EDTA (25-200-056), and L-Glutamine (25030081). Human breast adenocarcinoma MCF7 cell line (HTB-22), human breast adenocarcinoma MDA-MB-231 (HTB-26), and human breast adenocarcinoma MDA-MB-468 cell line (HTB-132), were purchased from American Type Culture Collection (ATCC, Manassas, VA). Agarose was obtained from Boston Bioproducts Inc. (P73050G, Ashland, MA). Paclitaxel (T7402) was purchased from Sigma-Aldrich (St. Louis, MO). Fetal bovine serum (FBS) was purchased from Atlanta Biologicals (Flowery Branch, GA) and type I rat collagen (3443-100-01) was purchased from R&D Systems (Minneapolis, MN).

2.1.2 | Immunohistochemistry

The following reagents needed for immunocytochemistry were purchased from Invitrogen (Carlsbad, CA): formalin, Goat serum, Triton-X, bovine serum albumin, phosphate-buffered saline, ProLong Gold Antifade Mountant. The anti-Ki-67 antibody (PA5-16785), anti-Caspase-3 antibody (700182), and citrate buffer were purchased from Thermo Fisher Scientific (BDB558615, Pittsburgh, PA). Vectastain elite ABC-HRP kit, DAB, Hematoxylin, and Bloxall solution were purchased from Vector laboratories (Burlingame, CA).

2.1.3 | 3D shear bioreactor components

The following materials and equipments were purchased for 3D shear bioreactor fabrication: polydimethylsiloxane (PDMS) elastomer and curing agent (Sylgard 184, Dow Corning, Midland, MI), polyethylene plugs (PEP; PE16030, SPC Technologies Ltd., Norfolk, UK), poly(methyl methacrylate; PMMA) (11510102, Astra Products, Copiague, NY), tubing (PharMed BPT, Saint Gobain, Akron, OH), and peristaltic pump (FH100, Thermo Fisher Scientific). The main bioreactor body was constructed from a $14 \times 14 \times 2$ cm acrylic block purchased and machined in the machine shop at the University of Michigan Physics department. The endplates were constructed from $6 \times 6 \times \frac{1}{2}$ inch aluminum plates and machined in house.

2.2 | Cell culture

Cells were cultured in 15 cm tissue culture-treated polystyrene plates using RPMI 1640 growth medium (MCF7 and MDA-MB-231) or DMEM growth medium (MDA-MB-468) supplemented with 10% FBS and 1x antibiotic/antimycotic until 80% confluency was reached. Cells were maintained routinely in tissue culture until they were ready to be harvested for use in the 3D bioreactor or 3D control gels.

2.3 | Construction and characterization of hydrogels

The interpenetrating network (IPN) hydrogel comprised of two components: agarose (3% w/v), and type I rat collagen ($500 \mu\text{g ml}^{-1}$, Fisher). Hydrogels were supplemented with 10% FBS. Cells were seeded within the liquid collagen/agarose solution at a density of 10 million/ml, before transfer to the bioreactor or control plate.

Methods for hydrogel characterization included scanning electron microscopy (SEM, Philips XL 30, SEMTech Solutions, MA), oscillatory rheometry (ARES, TA Instruments, New Castle, DE), and mercury porosimetry (Micromeritics Mercury Porosimeter Autopore V).

SEM characterization was performed for structural analysis of the network. Gels were first flash-frozen using liquid nitrogen then lyophilized (FreeZone 4.5 plus, Labconco, Kansas City, MO) for at least 24 hr before imaging with SEM.

Oscillatory rheometry was used to investigate the shear moduli of the IPN hydrogel. Tests were performed using 25 mm parallel plate geometry. Frequency sweeps were performed at 0.5% strain with a frequency ranging from 100 rad s^{-1} to 0.1 rad s^{-1} . The strain value for these tests was determined from strain sweeps performed at 0.3 Hz. The complex shear moduli, G^* , was calculated from the resulting storage modulus, G' , and loss modulus, G'' .

Mercury porosimetry (MicroActive AutoPore V9600 Version 1.02) was utilized for pore structure and permeability analysis of the IPN hydrogel. Both 3 and 5 cubic centimeter stem volumes were utilized at a mercury temperature of 18.93°C .

2.4 | 3D shear stress bioreactor

2.4.1 | Description

The 3D shear bioreactor was composed of a cell culture medium reservoir made from a modified IV bag that was fed through a peristaltic pump leading to the inlet of the bioreactor. The outlet of the bioreactor was connected back to the medium reservoir creating a continuous loop within the system. The layout of the 3D shear bioreactor flow circuit is depicted in Figure 1a. The bioreactor was machined from an acrylic block and consisted of eight hydrogel

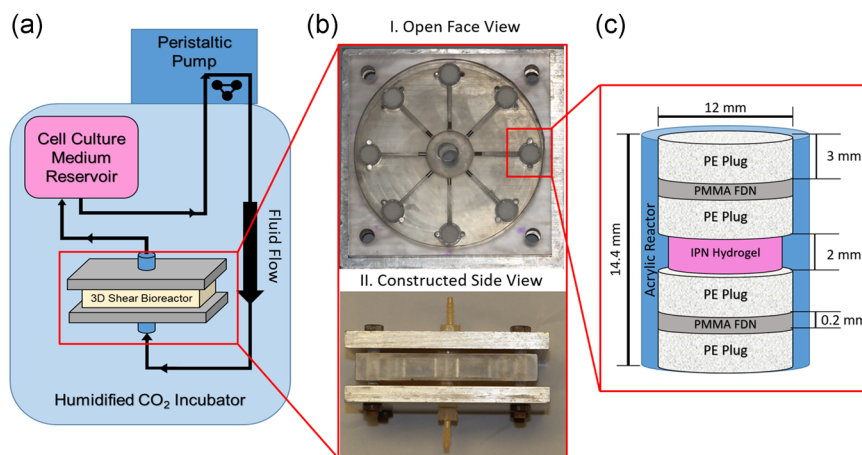


FIGURE 1 Schematic of the 3D shear stress bioreactor. (a) The layout of the shear bioreactor. The cell culture medium is contained in IV bag, pumped via a peristaltic pump into the bottom of the reactor, and recirculated into the cell culture medium reservoir, as indicated by the directional arrows in the schematic. (b) Photo of the disassembled (I) and assembled (II) bioreactor. (I) Flow plate showing radial flow chambers connecting the inlet of media flow to the cell-laden hydrogel stacks. (II) Constructed bioreactor, composed of flow plate with PDMS seals and steel endplates bolted together. (c) Schematic of interpenetrating (IPN) hydrogel stack composition and dimensions. Each stack was connected via a radial flow channel to both the inlet and outlet chamber. Hydrogel stack consisted of PE plug, PMMA fluid distribution net, PE plug sandwich surrounding cell-laden hydrogel to both hold the hydrogel in place and evenly distribute fluid flow. 3D, three-dimensional; PDMS, polydimethylsiloxane; PE, polyethylene; PMMA, poly(methyl methacrylate) [Color figure can be viewed at wileyonlinelibrary.com]

stacks positioned radially from an inlet flow chamber. The flow chambers were sealed with PDMS gaskets and held in place by two compressed aluminum plates. Images of the disassembled and assembled 3D bioreactor are shown in Figure 1b. Continuous and pulsatile cell culture medium flow was provided by a peristaltic pump at a volumetric flow rate of $2.28 \pm 0.035 \text{ ml s}^{-1}$. Cell culture medium was pumped through the inlet flow chamber, eight hydrogel stacks, then back out the collective exit. The hydrogel stacks were composed of 3D cell-laden agarose-collagen IPN gels (2 mm tall, 11.61 mm diameter) in a cylindrical column bordered by 3 mm thick PEP, 0.2 mm thick polymethyl methacrylate fluid distribution nets (PMMA-FDN), and the second set of 3 mm PEP all with a diameter of 12 mm. The smaller diameter gel allowed for a protective notch in the wall of the bioreactor, eliminating gel compression during plug insertion. The stack is depicted in Figure 1c. Shear stresses were modeled using COMSOL Multiphysics 5.3. A detailed description of the computational model is provided in Section 2.4.3.

2.4.2 | Preparation, assembly, and use

Before use, the bioreactor was washed and sterilized with a 24 hr ethylene oxide treatment at 54.4°C . All other components were sterilized by autoclaving, exposure to 70% ethanol, and 30 min UV treatment. The first half of the stack (PEP, PMMA FDN, PEP) was put in place, followed by the cell-laden hydrogel. The cells were concentrated and spun down to 10 million cells before suspension into the hydrogel. The cells and IPN hydrogel solution was polymerized within the bioreactor and conformed to the shape of the chamber (3 min, 25°C). After polymerization, the remaining portions of the stack (PEP, PMMA-FDN, PEP) were inserted on top of the hydrogel (Figure 1c). This was followed by placing 5 mm stainless steel rods within the flow chambers to control the velocity profile. PDMS gaskets (7 mm thick) were used to seal the bioreactor flow chambers and were compressed using bolted aluminum endplates. The inlet and outlet flow chambers were then attached to tubing, connecting the cell culture medium reservoir and pump to the bioreactor (Figure 1a). The bioreactor and cell culture medium reservoir were placed into the incubator (37°C , 5% CO_2) and the pump was started at a flow rate of $1.11 \text{ cm}^3 \text{ s}^{-1}$ before gradually increasing to $2.276 \text{ cm}^3 \text{ s}^{-1}$. Fluid flow was provided in a direction running vertically from the bottom to the top of each hydrogel stack.

Experiments were performed for 72 hr of continuous applied shear stress. Unstimulated control 3D gels, encapsulating cells were constructed to mimic the stimulated environment as completely as possible to ensure observed phenotypic changes were only attributed to shear stress stimulation within the bioreactor. The control gels were housed in 15 cm plates, submerged in 20 ml of cell culture medium and kept within equivalent incubation conditions for 72 hr (37°C , 5% CO_2). For drug experiments, paclitaxel was dissolved in the perfusate ($25 \mu\text{M}$) before the experimental start. Paclitaxel dosage of $25 \mu\text{M}$ was previously determined as an effective IC_{50} in 3D cell culture (Chen et al., 2013; Sarkar & Kumar, 2016). Each experimental

condition was repeated a minimum of three times with up to eight technical replicates.

2.4.3 | Computational analysis of shear stress

A numerical model was constructed of the 3D shear bioreactor using COMSOL Multiphysics 5.3 to estimated forces experienced within the hydrogel. Symmetry was used to simplify the model design. The cellular medium flow throughout the flow chambers and hydrogel stack were modeled utilizing Free and Porous Media Flow physics, as found in COMSOL and displayed in Equations (1–4).

$$\rho(u_3 \cdot \nabla)u_3 = \nabla \cdot [-pI + \mu(\nabla u_3 + (\nabla u_3)^T)] + F \quad (1)$$

$$\rho \nabla \cdot u_3 = 0 \quad (2)$$

$$0 = \nabla \cdot \left[-pI + \frac{\mu}{\epsilon_p}(\nabla u_3 + (\nabla u_3)^T) - \frac{2\mu}{3\epsilon_p}(\nabla \cdot u_3)I \right] - \left(\frac{\mu}{\kappa_{br}} + \beta_F |u_3| + Q_{br} \right) u_3 + F \quad (3)$$

$$\rho \nabla \cdot u_3 = Q_{br} \quad (4)$$

A second, sequential COMSOL model estimated the peak shear stresses experienced by a given cell within the hydrogel via laminar flow physics. The governing equations are shown below in Equations (5) and (6).

$$\rho(u \cdot \nabla)u = \nabla \cdot [-pI + \mu(\nabla u + (\nabla u)^T)] + F \quad (5)$$

$$\rho \nabla \cdot u = 0 \quad (6)$$

Equations (1) and (2) describe the Navier–Stokes equations for free-flowing medium and Equations (3) and (4) describe the Brinkman equation for porous media flow. Equations (5) and (6) describe the Navier–Stokes equation for freely moving fluid. The equation terms are defined as: ρ density, u velocity field, p pressure, I identity matrix, μ dynamic viscosity, T temperature, F external forces (e.g. gravity), ϵ_p porosity, κ_{br} permeability, β_F Forchheimer drag, and Q_{br} volumetric flow rate.

Values for the respective material properties were determined experimentally and included under Porous Matrix Properties. A hydrostatic water column was used to determine porosity values of PE and PMMA materials using Darcy's law of permeability (Hwang et al., 2010). Porosity was calculated from SEM images of the PE and hydrogel and light microscope images of the PMMA FDN on ImageJ. For accurate estimation of these values, measurements were repeated six or more times each for permeability and a minimum of three images were quantified for porosity estimations. The permeability of the hydrogel was estimated via mercury porosimeter studies. Material characteristic values are listed in Figure 2c.

Boundary layers were placed along all edges of the models to capture accurate fluid interfaces within the 3D bioreactor. A mesh analysis was performed to confirm the results were independent of

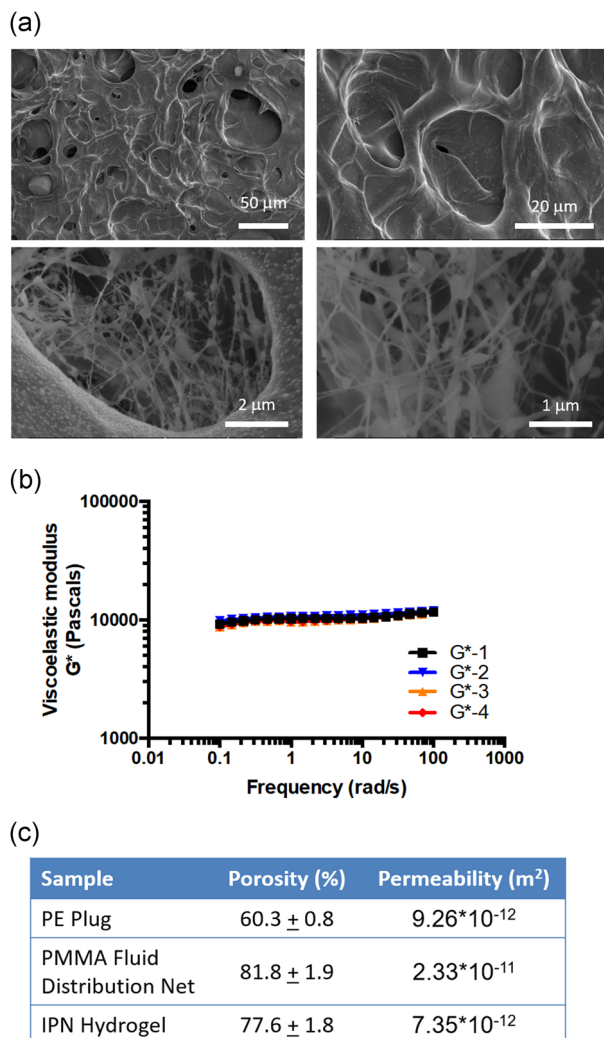


FIGURE 2 Material characterization of interpenetrating (IPN) hydrogel stack components. (a) SEM images of collagen/agarose IPN hydrogels in order of increasing magnification, where a reticulated network of collagen fibers was observed within a global agarose construct. (b) Graphical representation of a frequency sweep from rheometric testing of collagen/agarose IPN hydrogels. Four trials were utilized to determine the viscoelastic modulus of the IPN hydrogel, averaging 10358 ± 81.56 Pa. (c) Table of material properties for each component of the hydrogel stack. Values were determined by experimental measure through SEM analysis, ImageJ quantification, hydrostatic water column flow rate, and mercury porosimetry. SEM, scanning electron microscopy [Color figure can be viewed at wileyonlinelibrary.com]

mesh size (Figure S1). Model results are depicted in Figure 3. The primary model (Figure 3a–d) determines the average fluid velocity through the hydrogel. This value was subsequently used as input for the secondary model, simulating fluid flow around an idealized cell (Figure 3e). The resultant viscous shear stress was then recorded along the perimeter of the cell, where a maximum incident shear stress value was determined (Figure 3f; Ip et al., 2016).

In addition, hypoxic conditions within the gels were investigated within a COMSOL model. Neither the 3D control nor the 3D shear

stress IPN hydrogels demonstrated hypoxic conditions (Figure S2). Further details on the hypoxic COMSOL modeling conditions can be found in Supporting Information.

2.5 | Cell morphometry analysis

Slides were stained for Hematoxylin and Eosin (H&E) and imaged under a light microscope at 40× magnification for morphometry and shape factor analysis. These images were analyzed using ImageJ to quantify cellular area and circularity. A minimum of three biological replicates were analyzed each containing eight technical replicates. A minimum of 160 cells were quantified for each condition.

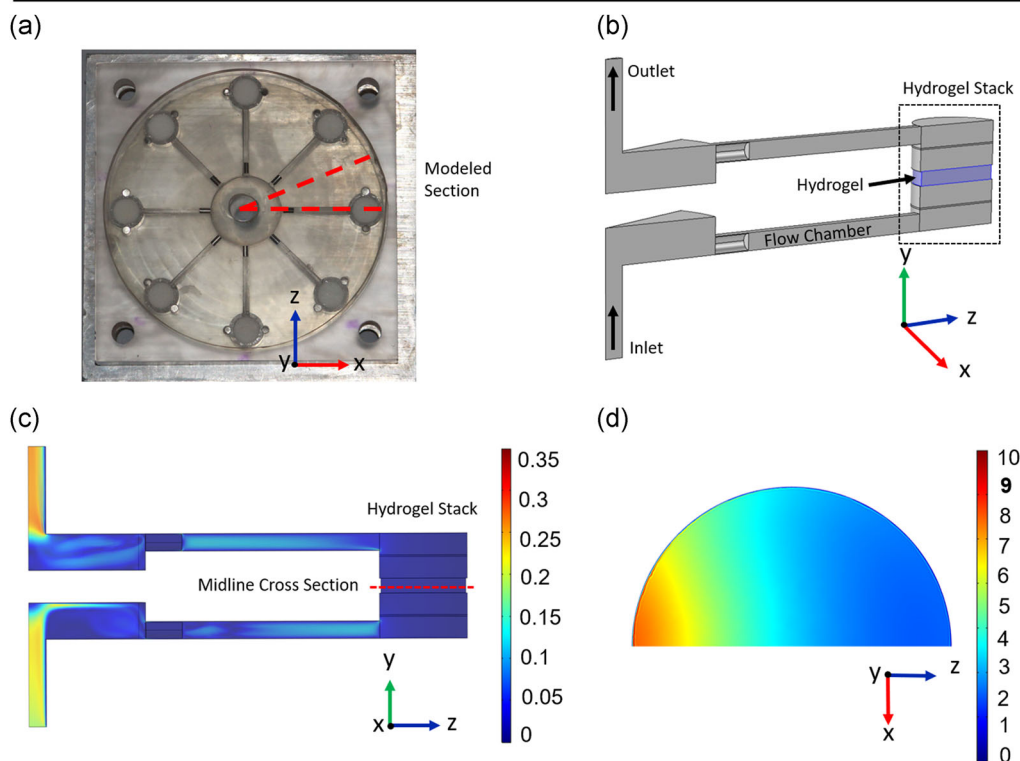
2.6 | Immunohistochemistry analysis

Cell laden hydrogels, once removed from the 3D shear bioreactor or control conditions were placed in 4% neutral buffered formalin, paraffin-embedded, and sectioned (perpendicular to the flow direction) in preparation for immunohistochemistry analysis. Briefly, slides were deparaffinized and boiled in citrate buffer for 20 min. Bloxall was used to quench endogenous peroxidase activity for 10 min before the application of blocking serum for 20 min. The primary antibody solution was incubated for 30 min followed by washing and secondary antibody incubation for 30 min. After washing, the ABC reagent was applied (30 min), slides were washed, and DAB was applied for approximately 1 min while slides were viewed under a digital inverted EVOS microscope to ensure adequate color contrast. Slides were then rinsed and counterstained with hematoxylin. Images were taken on an inverted Nikon E800 microscope and quantification of the resulting images was performed in ImageJ (ImageJ win64). Positive Ki67 or caspase 3 cells were counted and normalized to total cell counts within the image. Caspase 3 results were then normalized to nondrug treated controls for the respective cell line. A minimum of five images were taken per sample with a minimum of three experimental replicates analyzed per condition. Drug treated experimental results were normalized to control averages.

2.7 | Upregulation of gene expression in cells under shear stress

Total RNA was extracted from gels using an RNeasy Mini Kit (Qiagen, Valencia, CA). An additional buffer RPE wash step was amended to the manufacturer's protocol for enhanced purity. The RNA quality and quantification were assessed using a NanoDrop 1000 spectrophotometer (NanoDrop, Wilmington, DE). All samples used for quantitative polymerase chain reaction (qPCR) analysis passed RNA purity (260/280 and 260/230) with a ratio of 2.0 or better. Gene expression analysis was performed in 96 well plates using quantitative reverse transcription-PCR (qRT-PCR) on a 7900HT system; 96 well plates also included qPCR controls, a reverse transcription control, and a human genomic DNA contamination control. Fold change in gene expression between control and shear stress stimulated cells was determined using the $2^{-\Delta\Delta C_t}$ method (Livak & Schmittgen, 2001). Gene expression analysis was performed on three

Primary Model



Secondary Model

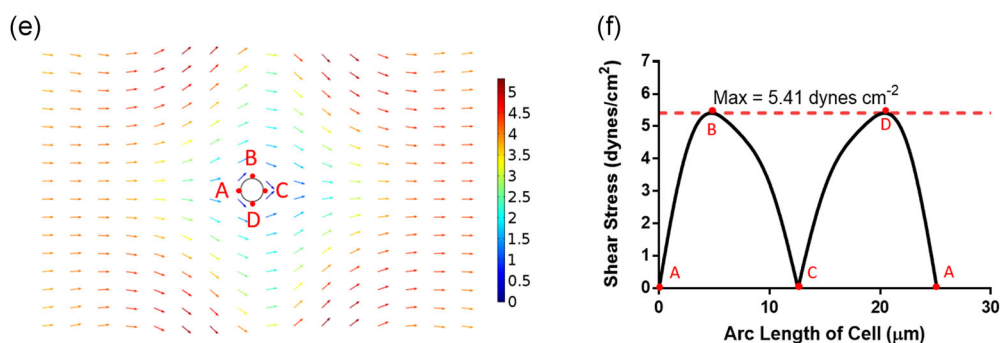


FIGURE 3 Finite element analysis of the 3D shear bioreactor quantifies shear stress. (a) Open face bioreactor with a dotted line denoting modeled section. (b) 3D COMSOL schematic of modeled section. IPN hydrogel highlighted in blue. (c) Flow velocity of the modeled section in m s^{-1} . Velocity ranges from 0 to 0.3 m s^{-1} along the surface of y - z plane. (d) Flow velocity in x - z plane of midline cross-section of the hydrogel in mm s^{-1} . (e) Secondary model of shear stress field experienced by a single cell within the IPN hydrogel. Average fluid velocity within the hydrogel, determined from the primary model (3C) was applied over an idealized spherical cell and resulting shear stress on the surface was determined. (f) Resulting shear stress around perimeter of cell within the flow field demonstrated in (e). Shear stress experienced by the cell is reported as the maximum value of $5.41 \text{ dyne cm}^{-2}$. 3D, three-dimensional; IPN, interpenetrating network [Color figure can be viewed at wileyonlinelibrary.com]

replicates within each cell type. Primer pairs utilized for qPCR PLAU expression were as follows: forward 5'-GGGAATGGTCACTTTTACC GAG-3', reverse 5'-GGGCATGGTACGTTTGCTG-3'.

2.8 | Urokinase activity assay and zymography

To quantify the level of urokinase-type plasminogen activator (urokinase, uPA) produced in the shear stressed experiments, a Chemicon uPA activity assay kit was performed on collected

phenol-free DMEM medium. All results were well within the sensitivity range of the uPA activity assay kit (0.05–50 units of uPA activity). In brief, the medium was collected from both shear stress and control gel experiments passed through a $0.22 \mu\text{m}$ PES sterilized filter, aliquoted, and stored in an -80°C freezer; $160 \mu\text{l}$ of sample was then added to a 96 well plate and incubated for 2 hr in combination with a pNA grouped tripeptide chromogenic substrate (determination of incubation period can be seen in Figure S3). Results were then quantified

using a microplate reader (BioTEK Synergy HT) at an absorbance reading of 405 nm.

Urokinase activity was additionally evaluated through zymography. Experimental media was concentrated 66.7-fold through 30 kDa centricon tubes (EMD Millipore, UFC703008) and was run at 100 V at room temperature. Zymography resolving gels were fabricated from DI water (9.575 ml), acrylamide (N,N'-Methylenebisacrylamide, 29:1) solution (5.025 ml), Tris buffer (1.5 M, pH 8.8, 5 ml), 8% milk solution (1.74 ml), and plasminogen (118.4 μ g) combined with SDS (10% w/v, 200 μ l), ammonium persulfate (10%, 200 μ l), and TEMED (8 μ l). Gels were then rinsed three times in triton-100 rinsing buffer (2.5% Triton X-100, 50 mM Tris-HCL pH 7.5, 0.05% NaN_3) for 10 min each. They were then incubated overnight in a renaturing buffer (0.1 M Glycine pH 8.0 adjusted with NaOH). Gels were rinsed in water three times for 5-min intervals, dyed with Simply Blue safestain for 1 hr, and rinsed in the water again. Destaining was then performed with methanol (30%), acetic acid (10%), and H_2O until band contrast was acceptable. Gel imaging was performed on the ChemiDoc™ Touch (BioRad, 732BR0111).

2.9 | Statistical analysis

All statistical analysis and graphical plots were derived in GraphPad Prism 6.0 (www.graphpad.com, San Diego, CA). All morphological data were calculated on ImageJ, and expressed as mean \pm SEM. All reported data are mean \pm SEM, derived from a minimum of three independent biological replicated experiments. Statistical comparison was performed using a one-way ANOVA for all data except the urokinase activity assay and zymography analysis where a two-tailed *t* test with Welch's correction was used.

3 | RESULTS

3.1 | Hydrogel characterization and finite element model

To ensure physiological representation of the pleural effusion TME, investigation of the hydrogel and bioreactor shear stress was performed. The biophysical characteristics of the collagen-agarose IPN hydrogel, showcasing fiber morphology, shear modulus, and porosity are illustrated in Figure 2. The reticulated network of collagen fibers within the agarose hydrogel is depicted in Figure 2a. The viscoelastic modulus of the IPN hydrogel was determined to be 10.36 ± 0.08 kPa (Figure 2b), was used in conjunction with Equation (7) to determine Young's modulus.

$$E = 2G(1 + \nu) \quad (7)$$

where, *E* is Young's modulus, *G* is viscoelastic modulus, and ν is Poisson's ratio. Poisson's ratio was estimated at 0.5, which is common for polymers such as equilibrium hydrated agarose hydrogels (Ahearne, Yang, Haj, Then, & Liu, 2005).

Modeling parameters utilized for COMSOL Multiphysics modeling were as follows (porosity, permeability): PE plug (60.3 ± 0.8 , 9.26×10^{-12} m^2); PMMA fluid distribution net (81.8 ± 1.9 , 2.33×10^{-11} m^2); IPN hydrogel (77.6 ± 1.8 , 7.35×10^{-12} m^2 ; Figure 2c). These values were then input into a finite element model using COMSOL Multiphysics (Figure 3).

Flow velocity within the simulated 3D hydrogel was output by the primary COMSOL model. Fluid flow velocity distribution at the center of the hydrogel is depicted in Figure 3d. The velocity of the cell culture medium in the x-z plane decreases in the IPN gel as the distance from the flow channel increases, however, flow velocity within the y-direction was uniform (Figure S1c). Fluid velocity within the entirety of the hydrogel was averaged and estimated as 3.83 mm s^{-1} . This value was then used as the input velocity of the secondary model to estimate the shear stress experienced by cells embedded within the hydrogel. An average cell size of 8 μm in diameter, as measured from the H&E stains, and spherical initial shape of the cell was assumed. From the model, the resulting maximum shear stress experienced by the cell surface was observed to be $5.41 \text{ dynes cm}^{-2}$.

3.2 | Shear stimulation significantly alters cellular morphology of breast cancer cells

Metastatic potential and invasive capability of cancer cells are often indicated through cellular morphology, thus shape factor analysis was performed. Cellular morphology of the shear stimulated cells were compared to 3D cultured controls. All cell types experiencing shear stress exhibited morphological changes including an increase in area and an elongated morphology (Figure 4a). These changes were quantified through ImageJ analysis and resulted in a significant increase in cellular area (MDA-MB-231: 1.2 fold, MDA-MB-468: 1.4 fold, MCF7: 1.8 fold) and a significant decrease in roundness (MDA-MB-231: 0.84 fold, MDA-MB-468: 0.90 fold, MCF7: 0.71 fold; Figure 4b,c). Perimeter and aspect ratio values were also determined to be significantly increased in all shear stressed breast cancer cells, whereas a significant decrease in circularity was found for MDA-MB-231 and MCF7 cell types (Figure S4).

3.3 | Breast cancer cellular proliferation increases with shear stress

To quantify the effect of shear stress on the proliferation of breast cancer cells, sections of the IPN hydrogel were immunohistochemistry (IHC) stained for Ki67 expression (hematoxylin counterstained) and quantified (Figure 5). Figure 5a shows representative images of control and shear stressed cells expressing Ki67. These results are graphically depicted in Figure 5b showing the fraction of proliferating cells more than doubling under shear stress for each cell type (MDA-MB-231: 2.5 fold, MDA-MB-468: 2.5 fold, MCF7: 5.0 fold).

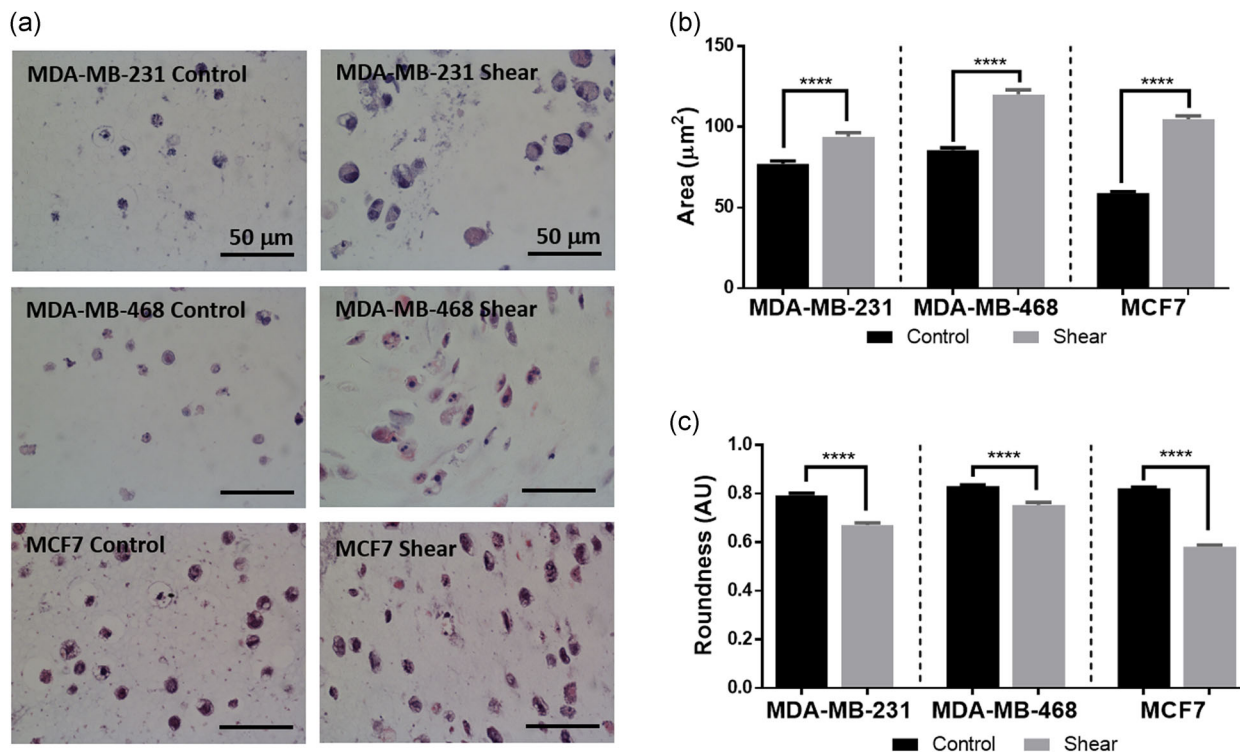


FIGURE 4 Shear stress increases area and decreases roundness in breast cancer cells. (a) Representative H&E images of shear and control studies for each cell type. Noticeable cellular elongation and increased cellular area are seen in all shear samples. All scale bars are 50 μm. (b) Graph of cellular area quantification comparing control and sheared cells. Shear stress exposure shows a significant increase in cellular area for all cell types (one-way analysis of variance [ANOVA] **** $p < .0001$, $n \geq 3$). (c) Quantification of cell roundness comparing control and sheared cells. Shear stress exposure shows a significant decrease in cell roundness for all cell types (one-way ANOVA **** $p < .0001$, $n \geq 3$). H&E, hematoxylin and eosin [Color figure can be viewed at wileyonlinelibrary.com]

3.4 | Breast cancer cells show chemoresistance while under shear stress stimulus

Given that mechanotransduction can modulate cellular responses to anti-neoplastic agents (Ip et al., 2016; McGrail, Kieu, & Dawson, 2014; McGrail, Kieu, Iandoli, & Dawson, 2015), breast cancer cells were treated with 25 μM paclitaxel for 72 hr. Chemotherapy treatment was administered at the previously determined IC_{50} concentration of 25 μM (Chen et al., 2013; Sarkar & Kumar, 2016). This concentration was sufficient to significantly increase cell death for all drug-treated controls when compared to nondrug treated controls (MDA-MB-231: 3.8 fold, MDA-MB-468: 1.5 fold, MCF7: 2.2 fold; Figure S5) as determined through IHC caspase 3 quantification. Under paclitaxel treatment, shear stressed cells remained more viable than their drug-treated control counterparts demonstrated as a significant reduction in cell death (Figure 6a,b).

In addition, proliferation analysis via Ki67 staining was performed on chemoresistance investigations. Proliferation remained significantly increased in drug-treated shear experiments when compared to drug-treated controls. Paclitaxel treatment seemed to have little effect on proliferation values as drug-treated shear experiments were significantly more proliferative than nondrug treated controls (Figure S5).

3.5 | Shear stimulation significantly upregulates *PLAU* gene expression

Changes in gene regulation due to shear stress stimulation were investigated for the identification of potential mechanotransduction pathways. Change in the gene expression of breast cancer cells, after stimulation with shear stress for 72 hr, was quantified using qRT-PCR. The *PLAU* gene was found to have a greater than 2-fold increase in RNA expression under shear stimulation when compared to controls for both MDA-MB-231 and MDA-MB-468 cell types. MDA-MB-231 cells increased *PLAU* expression 3.33 ± 0.89 -fold, MDA-MB-468 cells increased *PLAU* 3.567 ± 0.64 -fold, and MCF7 cells increased *PLAU* 1.08 ± 0.37 -fold (Figure 7a). All experimental runs are normalized to their respective controls, as such all control conditions result in a fold upregulation of 1.

3.6 | Protein expression confirms the enzymatic activity of urokinase

The *PLAU* gene encodes for the enzymatic protein urokinase which functions to degrade plasminogen into plasmin. It is a secreted protein present in all cells where it aids in the degradation of surrounding ECM to assist in cell migration/invasion. To investigate the protein expression of urokinase, both a commercially available

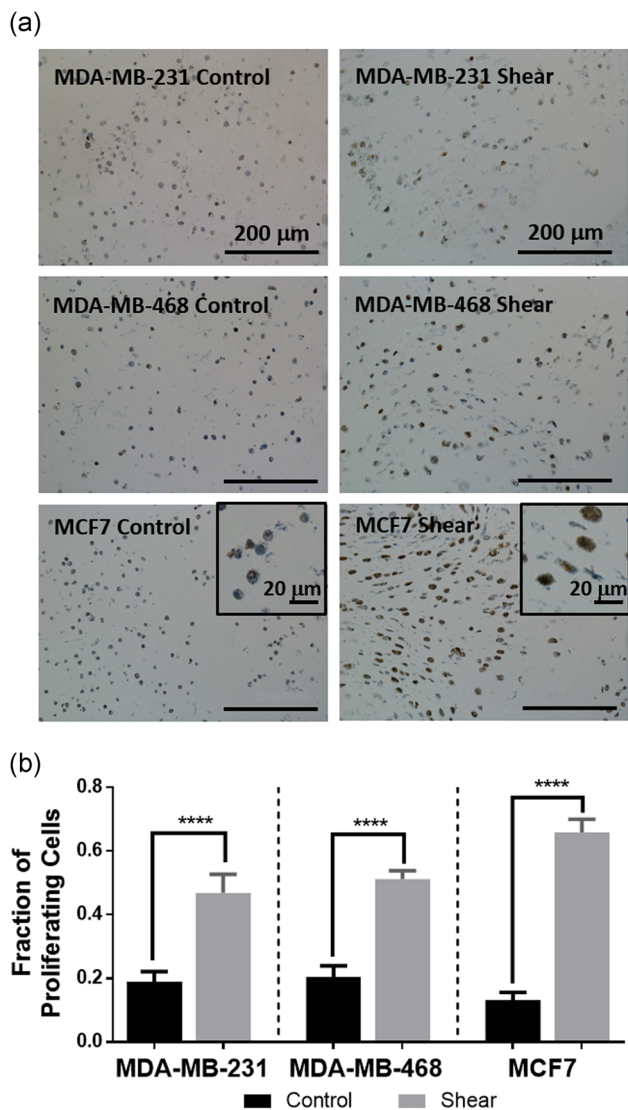


FIGURE 5 Shear stress increases breast cancer proliferation. (a) Representative images of Ki67 IHC counterstained with hematoxylin. Deep brown coloring indicates a proliferating cell and was quantified manually. Counts were normalized to total cell count within each image. Scale bars are 200 μm in the main images and 20 μm in the corner frames for MCF7 cells. (b) Graphical representation of the fraction of proliferating cells for each cell type under control and shear conditions (**** $p < .0001$, $n \geq 3$). All cell types show a significantly increased proliferation tendency under shear stress stimulus. IHC, immunohistochemistry [Color figure can be viewed at wileyonlinelibrary.com]

enzymatic activity assay and a plasminogen zymography test was performed. The experimental medium was collected after the completion of three 72-hr MDA-MB-468 experiments for use in protein/enzyme analysis. Shear stressed cells were discovered to have a significantly higher enzymatic activity of urokinase than the unstimulated controls (2.5 fold; Figure 7b). As a means for independent verification, zymography was performed on plasminogen acrylamide gels. After the conclusion of the trial, the experimental medium was concentrated and run in the zymography gel. The

resulting band intensity was normalized to its respective control. Shear stimulated MDA-MB-468 cells significantly increased secretion of uPA (1.4 fold; Figure 7c,d).

4 | DISCUSSION

Both cancer and nonmalignant cells experience shear stress in many microenvironments (Jain, Martin, & Stylianopoulos, 2014; Mitchell & King, 2013b; Shieh & Swartz, 2011). The inflammatory environment surrounding the tumor, as well as the structure of the TME, act to increase interstitial flow, thus increasing the shear stress experienced by cancer cells (Harrell et al., 2007; Mitchell & King, 2013b; Pedersen et al., 2010). This mechanical stimulus aids in cellular invasion while hindering chemotherapy delivery to the center of the tumor, resulting in chemoresistance and a flow gradient outwards from the tumor (Ip et al., 2016; Lunt, Fyles, Hill, & Milosevic, 2008; Netti, Berk, Swartz, Grodzinsky, & Jain, 2000; Wirtz, Konstantopoulos, & Searson, 2011). These findings emphasize the importance of mechanotransduction by shear stress within the TME.

A variety of methods to apply and study the effects of shear stress on cells have already been devised. However, many of these methods study the application of force on a monolayer culture (Avraham-Chakim et al., 2013; Blackman, García-Cardena, & Gimbrone Jr, 2002; Mitchell & King, 2013a; Zhao et al., 2014). Though 2D systems can apply uniform stimulation, these methods lack the physiologic 3D shear stress found within the TME. The 3D shear models currently in existence incorporate microfluidic design or single-cell analysis, which replicate the in vivo shear stress experienced by CTCs (Barnes et al., 2012; Ip et al., 2016). The constructs that investigate interstitial shear stress effects often only investigate migratory behaviors (Haessler, Teo, Foretay, Renaud, & Swartz, 2012) through microfluidics (Pola-check et al., 2011) and the use of Boyden chambers (Qazi, Shi, & Tarbell, 2011). While this type of device is advantageous for observation of small number of cells, it provides a hurdle for further downstream analysis such as western blot or qRT-PCR. In this report, we advance the existing shear bioreactor designs (Rotenberg et al., 2012) by: (a) incorporating a 3D IPN hydrogel that matches the morphology and modulus of the pleural effusion TME ECM, (b) embedding breast cancer cells within a 3D IPN hydrogel and providing variable pulsatile flow to the cells, (c) constructing a numerical model for a more accurate portrayal of fluid flow and shear stresses experienced by the breast cancer cells within the 3D bioreactor, and (d) increased yield of cells for molecular biology assays after experimental completion (not typical with microfluidic devices).

The agarose IPN hydrogel was chosen to provide a 3D microenvironment capable of easy stiffness modulation, encapsulation of cells, and blank background free of excess growth factor stimulation as to avoid excess signaling cues to the cells (Ulrich, Jain, Tanner, MacKay, & Kumar, 2010; Ulrich, Lee, Shon, Moon, & Kumar, 2011). The collagen type I component was included to provide a minimal and easily controlled adhesive signal for the cells within the network to sense the shear stress stimulation and due to its key role

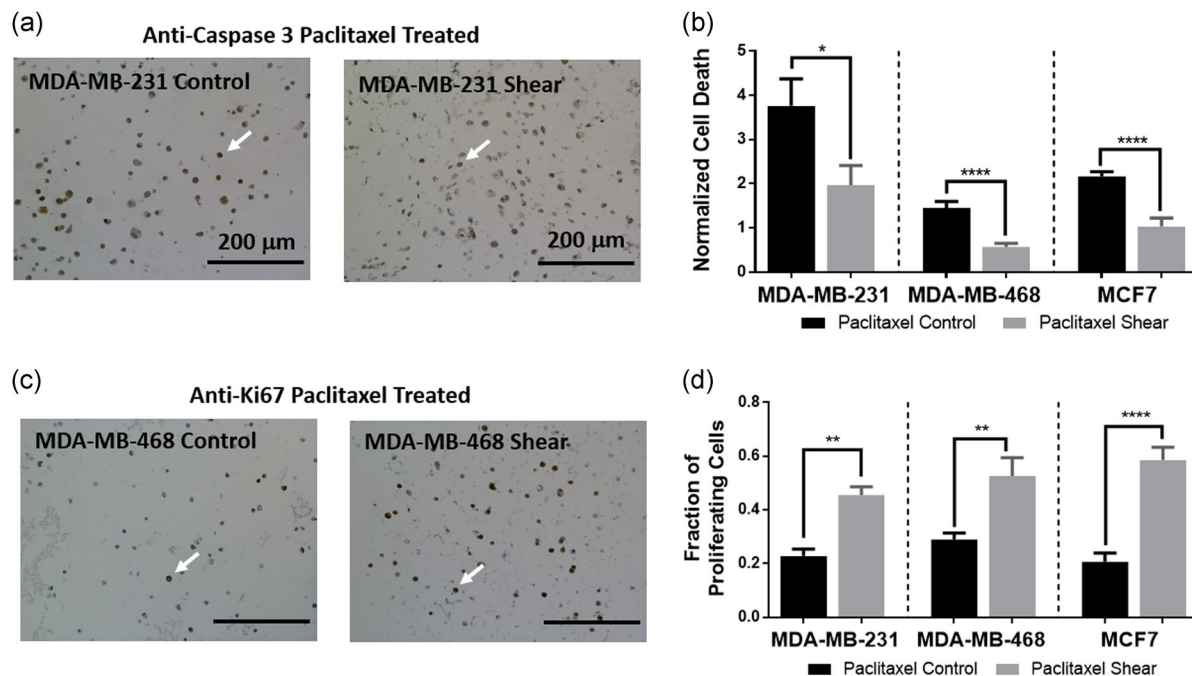


FIGURE 6 Shear stress-induced chemoresistance to paclitaxel treatment. (a) Representative images of caspase 3 IHC staining for MDA-MB-231 cells. Arrows indicate examples of cells positively expressing caspase 3. (b) Cells were treated with paclitaxel chemotherapy (25 μ M) in either control or shear conditions and cellular death was quantified using caspase 3 IHC staining, counterstained with hematoxylin. Results were manually quantified and compared to total cell number within the image. The fraction of proliferating cells was then normalized to the nonstimulated control average of the respective cell type. All cell types showed significantly decreased death under sheared conditions ($*p < .1$, $n \geq 3$). Three or more images were quantified for each experiment and a minimum of three biological replicates were performed for each condition. (c) Representative images of Ki67 IHC staining for MDA-MB-468 cells. Arrows indicate examples of cells positively expressing Ki67. (d) Cellular proliferation was analyzed using Ki67 IHC staining on paclitaxel treated experiments. Results were manually quantified, and each cell type showed significantly enhanced proliferation in sheared samples ($**p < .01$, $n \geq 3$). IHC, immunohistochemistry [Color figure can be viewed at wileyonlinelibrary.com]

within the breast cancer ECM (Ulrich et al., 2010, 2011). This hydrogel design has been previously utilized and investigated (Afrimzon et al., 2016; Lake, Hald, & Barocas, 2011; Ulrich et al., 2010, 2011). With this combination of IPN gel, cells could be encapsulated in situ within the bioreactor wells under highly regulated stiffness and adherence conditions. Normal breast tissue has been reported to have Young's modulus of approximately 3.25 kPa whereas breast tumors range from 6.41 to 42.52 kPa in stiffness depending on disease progression (Bae et al., 2018; Samani, Zubovits, & Plewes, 2007). The stiffness of the IPN agarose-collagen hydrogel fell well within this range attaining Young's modulus value of 31.08 kPa. At this stiffness, the IPN hydrogels most closely replicated intermediate to high grade infiltrating ductal carcinoma (Samani et al., 2007) and could be easily adjusted to suit alternate TME biophysical properties.

We developed a two-Step COMSOL model that enables greater accuracy when calculating estimated shear force experienced by cells captured within the 3D microenvironment. The first model uses a 3D rendering of the shear bioreactor to determine the fluid velocity and velocity distribution within the hydrogel. Subsequently, the estimated velocity is input as the inlet velocity for the secondary COMSOL model that applies the input flow over an ideal spherical cell. Due to the complicated IPN network, specific adhesive sites for the cell are not included, rather the shear velocity along the surface

is calculated and the maximum shear stress is reported. This two-step system is more comprehensive than previous models for similar bioreactors (Rotenberg et al., 2012) due to the inclusion of the entire continuous flow path within the bioreactor, as well as, all components of the hydrogel stack, which were found to be relevant in model results. While the majority of cells experience the same maximum shear value regardless of their vertical positioning within the hydrogel, there is some variation in flow velocity in the x-z plane. This is due to the location of the inlet flow chamber lateral to the hydrogel stack and respective flow distribution components. From these models, advanced estimates of cellular stimulation can be predicted with spatial accuracy within the hydrogel. The average shear stress values experienced by cells were determined to be 5.41 dynes cm^{-2} .

When exposed to shear stimulation in 2D, epithelial ovarian cancer cells have been shown to elongate and increase formation of stress fibers (Avraham-Chakim et al., 2013), whereas endothelial cells align in the direction of the shear force and elongate (Avraham-Chakim et al., 2013; Blackman et al., 2002). The cell morphological data from our breast cancer cell lines under shear stress are consistent with these outcomes. Similarly, several studies demonstrate alterations in gene expression related to proliferation when exposed to shear stress (Avraham-Chakim et al., 2013; Ip et al., 2016; Mitchell & King, 2013a; Yao, Rabodzey, & Dewey, 2007). The results of this

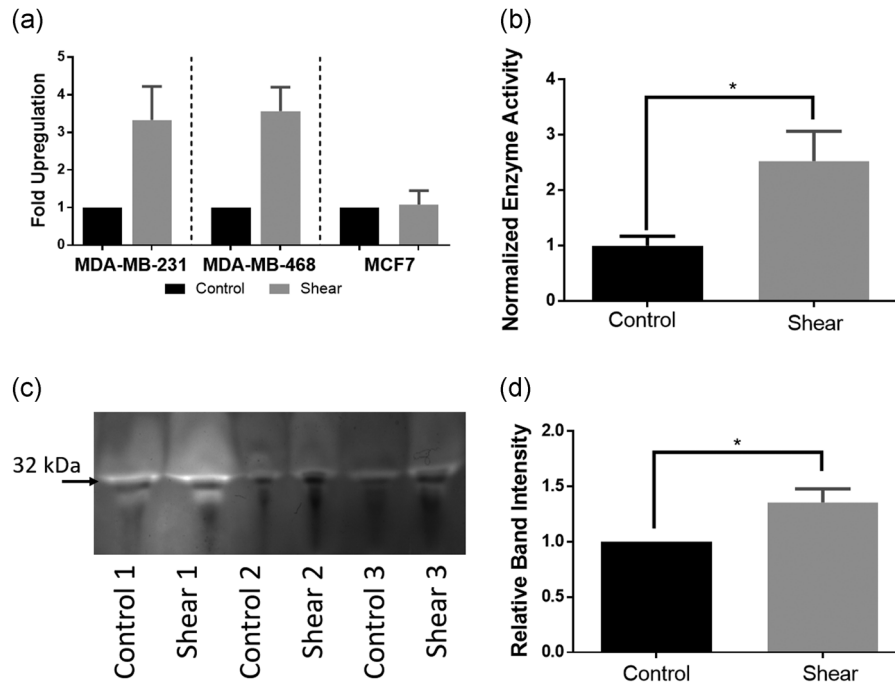


FIGURE 7 Activity assay and zymography confirm enhanced urokinase activity under shear stimulation. (a) qPCR analysis on PLAU expression showed significant upregulation for MDA-MB-231 ($*p < .1$, $n \geq 3$) and MDA-MB-468 ($**p < .01$, $n \geq 3$). MCF7 cells showed an increase in PLAU expression but were not significant ($n \geq 3$). (b) Confirmation of PLAU upregulation was performed using a urokinase activity assay on MDA-MB-468 experimental medium. Results showed a significant increase in enzymatic activity for shear samples normalized to controls. (c) Additional confirmation of urokinase protein activity was performed via plasminogen zymography. Band intensity for three MDA-MB-468 experimental sets is shown (32 kDa low molecular weight form uPA). (d) Quantification of the zymography band intensity was normalized to their respective controls and statistically analyzed with a two-tailed *t* test. MDA-MB-468 sheared samples showed a significant increase in band brightness, indicating increased urokinase enzyme activity. qPCR, quantitative polymerase chain reaction

study demonstrate that shear stress increases the proliferative ability of the breast cancer cells, whereas normal vascular endothelial cells have been found to inhibit proliferation in the presence of shear stress (Akimoto, Mitsumata, Sasaguri, & Yoshida, 2000).

Gene expression analysis showed a significant enhancement of PLAU under shear stimulation. The PLAU gene codes for uPA, a secreted protein initially found in its inactive form that is then cleaved for activation (Mahmood et al., 2018). This enzyme primarily activates plasminogen (proenzyme) to plasmin (multiple substrate cleaving enzyme; Rao, 2003). Plasmin then aids in the migratory cascade through degradation of ECM components, activation of MMPs, the release of growth factors, and functions as a feed-forward mechanism on the uPA-uPAR complex by activating pro-uPA to active uPA (Duffy, 2003; Duffy, McGowan, Harbeck, Thomssen, & Schmitt, 2014). Recently, uPA and its interactome have become a point of interest in cancer research due to its role in metastasis, proliferation, angiogenesis, its frequent aberrant expression within a variety of cancers, and its potential role as a diagnostic biomarker and therapeutic target (Duffy et al., 2014; Mahmood et al., 2018). Many alternative studies have tied the uPA system with cancer progression such as Huang and colleagues who found a significant decrease in tumor metastasis with uPA knockdown in MDA-MB-231 cells (Huang et al., 2010). In addition, shear stress has been identified as a driver of PLAU expression (Dolan et al., 2012; Essig &

Friedlander, 2003; Sokabe et al., 2004). However, to our knowledge, this is the first time the PLAU excess has been tied directly to shear stress stimulus in cancer. The enhancement of uPA expression found under shear stress stimulation suggests support of the metastatic cascade via mechanotransduction mechanisms. This result is further supported by the enhanced uPA enzyme activity produced by the shear stress stimulated cells and morphological changes indicating enhanced invasive potential, emphasizing the importance of mechanotransduction to the metastatic cascade.

Finally, we investigated whether breast cancer cells under shear stress show greater resistance to chemotherapy. Cells stimulated with shear stress were more resistant to paclitaxel treatment compared to unstimulated controls emphasizing the necessity to consider shear stress stimulus in treatment investigations. These findings are consistent with Ip et al. (2016) who tested paclitaxel treatment of ovarian cancer spheroids under shear stress finding enhanced drug resistance. When cellular proliferation was investigated simultaneously with drug treatment, little effect was found on the proliferating population despite paclitaxel's mechanism of action on cell division (Weaver, 2014). Overall, these findings reinforce the importance of recapitulating the *in vivo* mechanical microenvironments for fundamental and translational approaches.

The design of this shear bioreactor enables simultaneous 3D cell culture along with tunable shear stress that provides a physiologic

mechanical microenvironment for cancer biology investigations. Under these conditions more accurate results for in vitro modeling, drug screening, and therapeutic investigation for breast cancer can be realized. The versatility of this model provides a platform that can be applied to a multitude of cancer cell types and drug screening, enabling a better understanding of disease states and their responses.

5 | CONCLUSION

In conclusion, an improved 3D bioreactor capable of applying tunable shear stress to breast cancer cells within an IPN hydrogel matrix was designed and constructed. With the application of shear stress, morphological changes were observed in the breast cancer cells, including increased cellular area and decreased roundness. Shear stress stimulation also increased cellular proliferation and enhanced PLAU expression. Cells exposed to shear stress demonstrated higher resistance to chemotherapy treatment with paclitaxel, and the proliferation in this condition was unaffected. These findings demonstrate that breast cancer cells under shear stress stimulus adopt enhanced proliferation, invasion, and chemoresistant phenotypes, emphasizing the importance of shear stimulus in a 3D setting. This data reveals the role of PLAU in modulating shear stress-induced mechanotransduction in breast cancer cells and provide researchers with a new 3D platform for understanding the fundamentals of shear stress-induced mechanotransduction and evaluating prospective chemotherapeutics effectively and efficiently.

ACKNOWLEDGMENTS

This material is based upon work supported by the DOD OCRP Early Career Investigator Award W81XWH-13-1-0134 and DOD Pilot Award W81XWH-16-1-0426 (G. M.). This study was supported by grants from the Rivkin Center for Ovarian Cancer and the Michigan Ovarian Cancer Alliance (MIOCA). The research reported in this publication was supported by the National Cancer Institute of the National Institutes of Health under award number P30CA046592. C. M. N. is supported by the National Science Foundation Graduate Research Fellowship under Grant No. 1256260. The authors would like to acknowledge assistance received from Dr. Shreya Raghavan, Dr. Kristopher Inman, Emily Lin, Judy Pore, and Bingxin Yu.

CONFLICT OF INTERESTS

The authors declare that there is no conflict of interests.

DATA ACCESSIBILITY

The raw/processed data required to reproduce these findings can be requested by contacting the corresponding author, Dr. Geeta Mehta (mehtagee@umich.edu).

ORCID

Geeta Mehta  <http://orcid.org/0000-0001-5967-6425>

REFERENCES

- Afrimzon, E., Botchkina, G., Zurgil, N., Shafran, Y., Sobolev, M., Moshkov, S., ... Deutsch, M. (2016). Hydrogel microstructure live-cell array for multiplexed analyses of cancer stem cells, tumor heterogeneity and differential drug response at single-element resolution. *Lab on a Chip*, 16, 1047–1062.
- Ahearne, M., Yang, Y., Haj, A. J. E., Then, K. Y., & Liu, K. -K. (2005). Characterizing the viscoelastic properties of thin hydrogel-based constructs for tissue engineering applications. *Journal of the Royal Society Interface*, 2, 455–463.
- Akimoto, S., Mitsumata, M., Sasaguri, T., & Yoshida, Y. (2000). Laminar shear stress inhibits vascular endothelial cell proliferation by inducing cyclin-dependent kinase inhibitor p21Sdi1/Cip1/Waf1. *Circulation Research*, 86, 185–190.
- Avraham-Chakim, L., Elad, D., Zaretsky, U., Kloog, Y., Jaffa, A., & Grisaru, D. (2013). Fluid-flow induced wall shear stress and epithelial ovarian cancer peritoneal spreading. *PLoS One*, 8, e60965. <http://search.proquest.com.proxy.lib.umich.edu/docview/1330895410/abstract/8C897248438C4093PQ/1>
- Avvisato, C. L., Yang, X., Shah, S., Hoxter, B., Li, W., Gaynor, R., ... Byers, S. W. (2007). Mechanical force modulates global gene expression and beta-catenin signaling in colon cancer cells. *Journal of Cell Science*, 120, 2672–2682.
- Bae, S. J., Park, J. T., Park, A. Y., Youk, J. H., Lim, J. W., Lee, H. W., ... Jeong, J. (2018). Ex vivo shear-wave elastography of axillary lymph nodes to predict nodal metastasis in patients with primary breast cancer. *Journal of Breast Cancer*, 21, 190–196.
- Barnes, JM, Nauseef, JT, & Henry, MD. (2012). Resistance to fluid shear stress is a conserved biophysical property of malignant cells. *PLoS One*, 7, e50973.
- Bersini, S., Jeon, J. S., Dubini, G., Arrigoni, C., Chung, S., Charest, J. L., ... Kamm, R. D. (2014). A microfluidic 3D in vitro model for specificity of breast cancer metastasis to bone. *Biomaterials*, 35, 2454–2461.
- Blackman, B. R., García-Cardeña, G., & Gimbrone Jr, M. A. (2002). A new in vitro model to evaluate differential responses of endothelial cells to simulated arterial shear stress waveforms. *Journal of Biomechanical Engineering*, 124, 397–407.
- Bredemeier, M., Edimiris, P., Mach, P., Kubista, M., Sjöback, R., Rohlova, E., ... Kasimir-Bauer, S. (2017). Gene expression signatures in circulating tumor cells correlate with response to therapy in metastatic breast cancer. *Clinical Chemistry*, 63, 1585–1593.
- Butcher, D. T., Alliston, T., & Weaver, V. M. (2009). A tense situation: Forcing tumour progression. *Nature Reviews Cancer*, 9, 108–122.
- Chen, J., Wang, J., Chen, D., Yang, J., Yang, C., Zhang, Y., ... Dou, J. (2013). Evaluation of characteristics of CD44+CD117+ ovarian cancer stem cells in three dimensional basement membrane extract scaffold versus two dimensional monocultures. *BMC Cell Biology*, 14, 7.
- Diamond, S. L., Eskin, S. G., & McIntire, L. V. (1989). Fluid flow stimulates tissue plasminogen activator secretion by cultured human endothelial cells. *Science*, 243, 1483–1485.
- Dolan, J. M., Sim, F. J., Meng, H., & Kolega, J. (2012). Endothelial cells express a unique transcriptional profile under very high wall shear stress known to induce expansive arterial remodeling. *American Journal of Physiology-Cell Physiology*, 302, C1109–C1118.
- Duffy, M. J. (2003). The urokinase plasminogen activator system: Role in malignancy. *Current Pharmaceutical Design*, 10, 39–49. <http://www.eurekaselect.com/62195/article>
- Duffy, M. J., McGowan, P. M., Harbeck, N., Thomssen, C., & Schmitt, M. (2014). uPA and PAI-1 as biomarkers in breast cancer: Validated for

- clinical use in level-of-evidence-1 studies. *Breast Cancer Research*, 16, 428.
- DuFort, C. C., Paszek, M. J., & Weaver, V. M. (2011). Balancing forces: Architectural control of mechanotransduction. *Nature Reviews Molecular Cell Biology*, 12, 308–319.
- Essig, M., & Friedlander, G. (2003). Tubular shear stress and phenotype of renal proximal tubular cells. *Journal of the American Society of Nephrology*, 14, 335–355.
- Haessler, U., Teo, J. C. M., Foretay, D., Renaud, P., & Swartz, M. A. (2012). Migration dynamics of breast cancer cells in a tunable 3D interstitial flow chamber. *Integrative Biology*, 4, 401–409.
- Harrell, M. I., Iritani, B. M., & Ruddell, A. (2007). Tumor-induced sentinel lymph node lymphangiogenesis and increased lymph flow precede melanoma metastasis. *The American Journal of Pathology*, 170, 774–786.
- Huang, H.-Y., Jiang, Z.-F., Li, Q.-X., Liu, J.-Y., Wang, T., Zhang, R., ... Yang, A.-G. (2010). Inhibition of human breast cancer cell invasion by siRNA against urokinase-type plasminogen activator. *Cancer Investigation*, 28, 689–697.
- Hwang, C. M., Sant, S., Masaeli, M., Kachouie, N. N., Zamanian, B., Lee, S.-H., & Khademhosseini, A. (2010). Fabrication of three-dimensional porous cell-laden hydrogel for tissue engineering. *Biofabrication*, 2, 035003.
- Hyder, A. R., Baudoin, N. C., Brown, M. S., Stremler, M. A., Cimini, D., Davalos, R. V., & Schmelz, E. M. (2018). Fluid shear stress impacts ovarian cancer cell viability, subcellular organization, and promotes genomic instability. *PLoS One*, 13, e0194170.
- Ip, C. K. M., Li, S.-S., Tang, M. Y. H., Sy, S. K. H., Ren, Y., Shum, H. C., & Wong, A. S. T. (2016). Stemness and chemoresistance in epithelial ovarian carcinoma cells under shear stress. *Scientific Reports*, 6, 1–11. <http://www.ncbi.nlm.nih.gov/pmc/articles/PMC4887794/>
- Jain, R. K., Martin, J. D., & Stylianopoulos, T. (2014). The role of mechanical forces in tumor growth and therapy. *Annual Review of Biomedical Engineering*, 16, 321–346.
- Kawai, Y., Kaidoh, M., Yokoyama, Y., & Ohhashi, T. (2013). Cell surface F1/Fo ATP synthase contributes to interstitial flow-mediated development of the acidic microenvironment in tumor tissues. *American Journal of Physiology-Cell Physiology*, 305, C1139–C1150.
- Lake, S. P., Hald, E. S., & Barocas, V. H. (2011). Collagen-agarose co-gels as a model for collagen-matrix interaction in soft tissues subjected to indentation. *Journal of Biomedical Materials Research*, 99A, 507–515.
- Li, Q., Chen, C., Kapadia, A., Zhou, Q., Harper, M. K., Schaack, J., & Labarbera, D. V. (2011). 3D models of epithelial-mesenchymal transition in breast cancer metastasis: High-throughput screening assay development, validation, and pilot screen. *Journal of Biomolecular Screening*, 16, 141–154.
- Livak, K. J., & Schmittgen, T. D. (2001). Analysis of relative gene expression data using real-time quantitative PCR and the 2- $\Delta\Delta$ CT method. *Methods*, 25, 402–408.
- Loessner, D., Stok, K. S., Lutolf, M. P., Hutmacher, D. W., Clements, J. A., & Rizzi, S. C. (2010). Bioengineered 3D platform to explore cell-ECM interactions and drug resistance of epithelial ovarian cancer cells. *Biomaterials*, 31, 8494–8506.
- Lunt, S. J., Fyles, A., Hill, R. P., & Milosevic, M. (2008). Interstitial fluid pressure in tumors: Therapeutic barrier and biomarker of angiogenesis. *Future Oncology*, 4, 793–802.
- Mahmood, N., Mihalciou, C., & Rabbani, S. A. (2018). Multifaceted role of the urokinase-type plasminogen activator (uPA) and its receptor (uPAR): Diagnostic, prognostic, and therapeutic applications. *Frontiers in Oncology*, 8, 1–21. <https://www.frontiersin.org/articles/10.3389/fonc.2018.00024/full>
- McGrail, D. J., Kieu, Q. M. N., & Dawson, M. R. (2014). The malignancy of metastatic ovarian cancer cells is increased on soft matrices through a mechanosensitive Rho-ROCK pathway. *Journal of Cell Science*, 127, 2621–2626.
- McGrail, D. J., Kieu, Q. M. N., Iandoli, J. A., & Dawson, M. R. (2015). Actomyosin tension as a determinant of metastatic cancer mechanical tropism. *Physical Biology*, 12, 026001.
- Mitchell, M. J., & King, M. R. (2013a). Fluid shear stress sensitizes cancer cells to receptor-mediated apoptosis via trimeric death receptors. *New Journal of Physics*, 15, 015008.
- Mitchell, M. J., & King, M. R. (2013b). Computational and experimental models of cancer cell response to fluid shear stress. *Frontiers in Oncology*, 3, 1–11. <http://journal.frontiersin.org/article/10.3389/fonc.2013.00044/abstract>.
- Munson, J. M., & Shieh, A. C. (2014). Interstitial fluid flow in cancer: Implications for disease progression and treatment. *CMAR*, 6, 317–328.
- Netti, P. A., Berk, D. A., Swartz, M. A., Grodzinsky, A. J., & Jain, R. K. (2000). Role of extracellular matrix assembly in interstitial transport in solid tumors. *Cancer Research*, 60, 2497–2503.
- Papadaki, M., Ruef, J., Nguyen, K. T., Li, F., Patterson, C., Eskin, S. G., ... Runge, M. S. (1998). Differential regulation of protease activated receptor-1 and tissue plasminogen activator expression by shear stress in vascular smooth muscle cells. *Circulation Research*, 83, 1027–1034.
- Patil, C. B., Gupta, A., Gupta, R., Dixit, R., Gupta, N., & Indushekar, V. (2015). Carcinoma breast related metastatic pleural effusion: A thoracoscopic approach. *Clinical Cancer Investigation Journal*, 4, 633.
- Pedersen, J. A., Boschetti, F., & Swartz, M. A. (2007). Effects of extracellular fiber architecture on cell membrane shear stress in a 3D fibrous matrix. *Journal of Biomechanics*, 40, 1484–1492.
- Pedersen, J. A., Lichter, S., & Swartz, M. A. (2010). Cells in 3D matrices under interstitial flow: Effects of extracellular matrix alignment on cell shear stress and drag forces. *Journal of Biomechanics*, 43, 900–905.
- Polacheck, W. J., Charest, J. L., & Kamm, R. D. (2011). Interstitial flow influences direction of tumor cell migration through competing mechanisms. *Proceedings of the National Academy of Sciences of the United States of America*, 108, 11115–11120.
- Polacheck, W. J., German, A. E., Mammoto, A., Ingber, D. E., & Kamm, R. D. (2014). Mechanotransduction of fluid stresses governs 3D cell migration. *Proceedings of the National Academy of Sciences of the United States of America*, 111, 2447–2452.
- Qazi, H., Shi, Z.-D., & Tarbell, J. M. (2011). Fluid shear stress regulates the invasive potential of glioma cells via modulation of migratory activity and matrix metalloproteinase expression. *PLoS One*, 6, e20348.
- Rao, J. S. (2003). Molecular mechanisms of glioma invasiveness: The role of proteases. *Nature Reviews Cancer*, 3, 489–501.
- Regmi, S., Fu, A., & Luo, K. Q. (2017). High shear stresses under exercise condition destroy circulating tumor cells in a microfluidic system. *Scientific Reports*, 7, 39975.
- Rijal, G., & Li, W. (2016). 3D scaffolds in breast cancer research. *Biomaterials*, 81, 135–156.
- Rizvi, N. A., Hellmann, M. D., Snyder, A., Kvistborg, P., Makarov, V., Havel, J. J., ... Chan, T. A. (2015). Mutational landscape determines sensitivity to PD-1 blockade in non-small cell lung cancer. *Science*, 348, 124–128.
- Rotenberg, M. Y., Ruvinov, E., Armoza, A., & Cohen, S. (2012). A multi-shear perfusion bioreactor for investigating shear stress effects in endothelial cell constructs. *Lab on a Chip*, 12, 2696–2703.
- Samani, A., Zubovits, J., & Plewes, D. (2007). Elastic moduli of normal and pathological human breast tissues: An inversion-technique-based investigation of 169 samples. *Physics in Medicine and Biology*, 52, 1565–1576.
- Sarkar, J., & Kumar, A. (2016). Thermo-responsive polymer aided spheroid culture in cryogel based platform for high throughput drug screening. *The Analyst*, 141, 2553–2567.
- Sepiashvili, L., Hui, A., Ignatchenko, V., Shi, W., Su, S., Xu, W., ... Kislinger, T. (2012). Potentially novel candidate biomarkers for head and neck squamous cell carcinoma identified using an integrated cell

- line-based discovery strategy. *Molecular & Cellular Proteomics*, 11, 1404–1415.
- Shieh, A. C., Rozansky, H. A., Hinz, B., & Swartz, M. A. (2011). Tumor cell invasion is promoted by interstitial flow-induced matrix priming by stromal fibroblasts. *Cancer Research*, 71, 790–800.
- Shieh, A. C., & Swartz, M. A. (2011). Regulation of tumor invasion by interstitial fluid flow. *Physical Biology*, 8, 015012.
- Siegel, R. L., Miller, K. D., & Jemal, A. (2018). Cancer statistics, 2018. *CA: A Cancer Journal for Clinicians*, 68, 7–30.
- Sokabe, T., Yamamoto, K., Ohura, N., Nakatsuka, H., Qin, K., Obi, S., ... Ando, J. (2004). Differential regulation of urokinase-type plasminogen activator expression by fluid shear stress in human coronary artery endothelial cells. *American Journal of Physiology-Heart and Circulatory Physiology*, 287, H2027–H2034.
- Sung, K. E., Su, X., Berthier, E., Pehlke, C., Friedl, A., & Beebe, D. J. (2013). Understanding the impact of 2D and 3D fibroblast cultures on in vitro breast cancer models. *PLoS One*, 8, e76373.
- Swartz, M. A., & Lund, A. W. (2012). Lymphatic and interstitial flow in the tumour microenvironment: Linking mechanobiology with immunity. *Nature Reviews Cancer*, 12, 210–219.
- Tang, L., & Han, X. (2013). The urokinase plasminogen activator system in breast cancer invasion and metastasis. *Biomedicine & Pharmacotherapy*, 67, 179–182.
- Triantafyllou, U. L., Park, S., Klaassen, N. L., Raddatz, A. D., & Kim, Y. (2017). Fluid shear stress induces cancer stem cell-like phenotype in MCF7 breast cancer cell line without inducing epithelial to mesenchymal transition. *International Journal of Oncology*, 50, 993–1001. <http://www.spandidos-publications.com/10.3892/ijo.2017.3865/abstract>
- Ulrich, T. A., Jain, A., Tanner, K., MacKay, J. L., & Kumar, S. (2010). Probing cellular mechanobiology in three-dimensional culture with collagen-agarose matrices. *Biomaterials*, 31, 1875–1884.
- Ulrich, T. A., Lee, T. G., Shon, H. K., Moon, D. W., & Kumar, S. (2011). Microscale mechanisms of agarose-induced disruption of collagen remodeling. *Biomaterials*, 32, 5633–5642.
- Waters, C. M., Glucksberg, M. R., Depaola, N., Chang, J., & Grotberg, J. B. (1996). Shear stress alters pleural mesothelial cell permeability in culture. *Journal of Applied Physiology*, 81, 448–458.
- Weaver, B. A. (2014). How Taxol/paclitaxel kills cancer cells. *MBoC*, 25, 2677–2681.
- Weigelt, B., Ghajar, C. M., & Bissell, M. J. (2014). The need for complex 3D culture models to unravel novel pathways and identify accurate biomarkers in breast cancer. *Advanced Drug Delivery Reviews*, 69, 42–51.
- Weinbaum, S., Cowin, S. C., & Zeng, Y. (1994). A model for the excitation of osteocytes by mechanical loading-induced bone fluid shear stresses. *Journal of Biomechanics*, 27, 339–360.
- Wirtz, D., Konstantopoulos, K., & Searson, P. C. (2011). The physics of cancer: The role of physical interactions and mechanical forces in metastasis. *Nature Reviews Cancer*, 11, 512–522.
- Xiong, N., Li, S., Tang, K., Bai, H., Peng, Y., Yang, H., ... Liu, Y. (2017). Involvement of caveolin-1 in low shear stress-induced breast cancer cell motility and adhesion: Roles of FAK/Src and ROCK/p-MLC pathways. *Biochimica et Biophysica Acta (BBA) - Molecular Cell Research*, 1864, 12–22.
- Yang, H., Guan, L., Li, S., Jiang, Y., Xiong, N., Li, L., ... Liu, Y. (2016). Mechanosensitive caveolin-1 activation-induced PI3K/Akt/mTOR signaling pathway promotes breast cancer motility, invadopodia formation and metastasis in vivo. *Oncotarget*, 7, 16227–16247.
- Yao, Y., Rabodzey, A., & Dewey, C. F. (2007). Glycocalyx modulates the motility and proliferative response of vascular endothelium to fluid shear stress. *American Journal of Physiology-Heart and Circulatory Physiology*, 293, H1023–H1030.
- Zhao, F., Li, L., Guan, L., Yang, H., Wu, C., & Liu, Y. (2014). Roles for GP IIb/IIIa and $\alpha v \beta 3$ integrins in MDA-MB-231 cell invasion and shear flow-induced cancer cell mechanotransduction. *Cancer Letters*, 344, 62–73.

SUPPORTING INFORMATION

Additional supporting information may be found online in the Supporting Information section.

How to cite this article: Novak CM, Horst EN, Taylor CC, Liu CZ, Mehta G. Fluid shear stress stimulates breast cancer cells to display invasive and chemoresistant phenotypes while upregulating PLAU in a 3D bioreactor. *Biotechnology and Bioengineering*. 2019;116:3084–3097. <https://doi.org/10.1002/bit.27119>